International Journal of Thermophysics, Vol. 20, No. 3, 1999

Vapor–Liquid Equilibria of Silicon by the Gibbs Ensemble Simulation[1]

N. Honda[2] and Y. Nagasaka[2, 3]

Vapor–liquid equilibrium simulations of silicon were performed using the Stillinger–Weber potential with the Gibbs ensemble Monte Carlo method (GEMC). In the low temperature region, from about 3000 to 3500 K, our calculations show the stability of phases and good agreement with several experimental results. On the whole, there is little dependence on the size of the system except near the estimated critical point of silicon: $T_c = 7500 \pm 500$ K and $\rho_c = 750 \pm 100$ kg · m^{-3} as determined by the law of rectilinear diameter. Above 3500 K, vapor–liquid coexistence properties which have not been obtained by experiment are derived.

KEY WORDS: critical point; Gibbs ensemble; silicon; simulations; vapor–liquid equilibria

1. INTRODUCTION

Until recently, little has been known about vapor–liquid coexistence properties of high-temperature melts and their vapor–liquid critical behavior. One of the reasons for this is that, under such conditions, experiments become extremely difficult and experimental measurements are not always possible. However, current industrial demands concerning high temperature and high pressure are expanding, so basic thermophysical properties, for example, the critical temperature and critical density, will be essential for these purposes even if they are difficult, or nearly impossible, to measure.

[1] Paper presented at the Thirteenth Symposium on Thermophysical Properties, June 22–27, 1997, Boulder, Colorado, U.S.A.

[2] Department of Mechanical Engineering, Keio University, 3-14-1, Hiyoshi Kohoku-ku, Yokohama 223, Japan.

[3] To whom correspondence should be addressed.

0195-928X/99/0500-0837$16.00/0

On the other hand, the calculational power of computers is accelerating so rapidly that simulations for complex systems and models that were previously unattainable are now possible. So the estimation of properties at high temperatures and high pressures by a variety of molecular simulations has become more and more useful and efficient.

Up to the present time, several simulation techniques have been developed for phase equilibria. The NPT-μ method [1, 2] is a conventional and empirical way to obtain saturated densities, chemical potentials, and the phase diagram of the fluid. The following new techniques, the Gibbs–Duhem integration method [3] and Gibbs ensemble Monte Carlo (GEMC) method [4], are presented as more efficient techniques. Among these methods, the GEMC is the only direct technique which does not assume any preliminary imformation except for knowledge concerning the interaction of the substances investigated. In particular, we have very few experimental and calculated data available in this study. In such a case, the GEMC seems to be the most suitable and effective methodology.

These methods have been mainly used and refined in the chemical engineering field. But in order to take advantage of the strength of simulations, systems which cannot be realized by experiments are a good application. For example, for high-temperature melts already performed by the GEMC, the restricted primitive model (RPM) by Panagiotopoulos [5] is available. This paper gives the vapor–liquid coexistence curve of NaCl in the very high-temperature region, from 1000 to 3200 K, and gives an estimate of the critical temperature of NaCl. This is a good example of using the advantages of simulations effectively.

Liquid silicon, a high-temperature melt, in which we are interested in this study, has considerable industrial and scientific interest. In spite of being one of the most abundant elements on earth, the behavior of silicon at high temperature is not accurately known due to its extremely high melting point (1687 K) and boiling point (3560 K) [6]. To our knowledge, there are no reliable data for its critical parameters. In this study, we attempt to use simulations to predict the high temperature vapor–liquid coexistence properties of silicon.

2. SIMULATION PROCEDURE

2.1. The Stillinger-Weber Potential

We used the Stillinger–Weber (SW) potential [7] as the model for silicon molecular interactions. There have been many efforts to develop a reliable potential model for silicon, but many of them were applied to the crystalline phase. Stillinger and Weber proposed the first model, which is

parameterized by considering not only the crystalline phase, but also the liquid silicon properties. This is an empirical model and has been widely used for the simulation of silicon including liquid and vapor phases, for example, cluster analysis [8], and the interface between solid and liquid [9]. This potential, consisting of the sum of two- and three-body interactions, seems to be adequate for our study.

Stillinger and Weber introduced three-body interaction terms in addition to the pair-interaction terms to stabilize the diamond structure. The overall expressions are given in the following form:

$$\phi = \sum_{i=1}^{N} \sum_{j=i+1}^{N} \phi_{ij} + \sum_{i=1}^{N} \sum_{j=i+1}^{N} \sum_{k=j+1}^{N} \phi_{ijk} \tag{1}$$

$$\phi_{ij}(r_{ij}) = \varepsilon f\left(\frac{r_{ij}}{\sigma}\right) \tag{2}$$

$$\phi_{ijk}(\mathbf{r}_i, \mathbf{r}_j, \mathbf{r}_k) = \varepsilon g\left(\frac{\mathbf{r}_i}{\sigma}, \frac{\mathbf{r}_j}{\sigma}, \frac{\mathbf{r}_k}{\sigma}\right) \tag{3}$$

$$f(x) = \begin{cases} A\left(\dfrac{B}{x^p} - \dfrac{1}{x^q}\right) \exp\left(\dfrac{1}{x-a}\right), & x < a \\ 0, & x \geqslant a \end{cases} \tag{4}$$

$$g(\mathbf{x}_i, \mathbf{x}_j, \mathbf{x}_k) = h(x_{ij}, x_{ik}, \theta_{jik}) + h(x_{ji}, x_{jk}, \theta_{ijk}) + h(x_{ki}, x_{kj}, \theta_{ikj}) \tag{5}$$

$$h(x_{ij}, x_{ik}, \theta_{jik}) = \begin{cases} \lambda \exp\left(\dfrac{\gamma}{x_{ij}-a} + \dfrac{\gamma}{x_{ik}-a}\right)\left(\cos\theta_{jik} + \dfrac{1}{3}\right)^2 \\ 0, \quad x_{ij} < a \quad \text{and} \quad x_{ij} < a \\ \qquad x_{ij} > a \quad \text{or} \quad x_{ik} < a \end{cases} \tag{6}$$

where A, B, p, q, and λ are adjustable parameters and each term vanishes if either r_{ij} or r_{jk} is greater than a and θ_{jik} is the angle between r_{ij} and r_{ik} subtended at vertex i. The angular term goes to zero at the ideal tetrahedral angle, about 108°. The set of parameter is given in Table I, and the pair potential of silicon in shown in Fig. 1. In calculating the phase equilibria, we assumed that this interaction potential will be used for silicon vapor as well as for liquid.

2.2. Computational Procedure

The system is assumed to consist of two bulk cells with cubic periodic boundary conditions. First, we placed a total of 128 or 250 particles in a simple lattice cube for all the simulations and initiated constant NVT

Table I. Potential Parameters in Eqs. (1)–(6) from Ref. 7.

ε(J)	3.4723×10^{-19}
σ(m)	2.0951×10^{-10}
A	7.049556277
B	0.6022245584
p	4
q	0
a	1.8
λ	21.0
γ	1.2

Gibbs calculations. Since a detailed explanation of the methodology is reported in Ref. 4, it is omitted here.

One of the most useful advantages of the GEMC is to be able to perform calculations without a prior knowledge of the thermophysical or chemical properties of the system. To start the simulations, all that is needed are two equal and intermediate densities. But to accelerate the convergence, this method may be less efficient. The more efficient way will be to fill some gaps to the regions in advance.

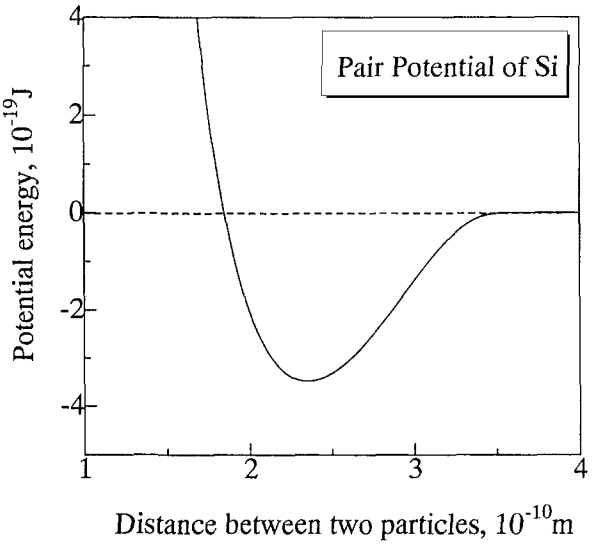

Fig. 1. Pair potential term of Stillinger–Weber potential referred to in Table I.

In our calculations, no numerical correction for potential energy change was taken into account. For the Lennard–Jones potential, the interaction is essentially defined at infinite distance. Thus, the truncated area is introduced, for example, $L/2$ or three or four times the parameter σ is commonly used in order to perform time-saving simulations. On the other hand, the SW potential terms vanish at a very short distance, 1.8σ. Thus, a truncation of potential and long-range correction is needed. We assume that this treatment is valid, and no calculation error will be generated using this approximation.

The calculation of chemical potential was performed using the conventional Widom equation for a test of our simulations. An inserted position was chosen at random in the region from the particle interchange step of the Gibbs method, and from the energy change derived from this step, a chemical potential μ can be calculated as follows:

$$\mu = k_B T \ln(\rho \Lambda^3) - k_B T \ln\langle \exp(-\Delta U/k_B T)\rangle \tag{7}$$

where k_B is the Boltzmann constant and Λ is the de Broglie wavelength.

For the system where two distinct phases coexist, the equality of chemical potentials between the two regions, $\mu^I = \mu^{II}$, should be satisfied. The calculated chemical potentials of the vapor and liquid phases agreed well. These results demonstrate that our SW systems obtained by the GEMC simulations satisfy thermodynamic conditions and that our assumption of vapor atoms, as mentioned above, did not have a fundamental error.

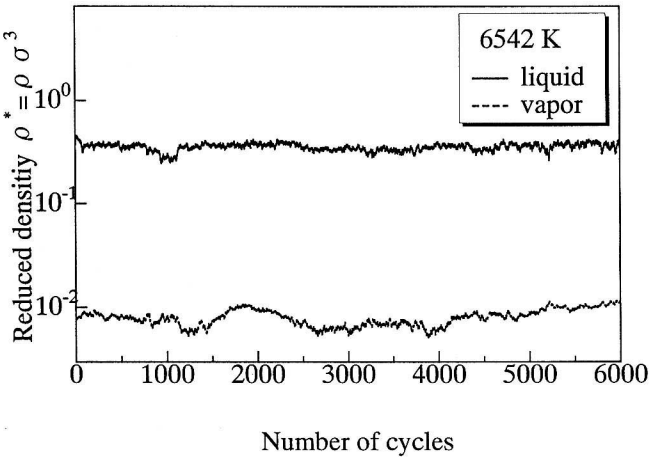

Fig. 2. Reduced density $\rho^* = \rho\sigma^3$ versus the number of cycles for the system of 250 particles for the SW potential at 6542 K ($T^* = 0.260$). One cycle consists of three types of trial moves, particle displacements, volume rearrangements, and particle interchanges.

The evolution of densities of the two phases as a function of the configurations is presented in Fig. 2 at $T = 6542$ K ($T^* = k_B T/\varepsilon = 0.260$). More than 7×10^5 configurations are generated in this calculation. The total number of particles of the two regions is 250 for the calculations shown in Fig. 2. The initial densities of the two phases were taken as those expected at the end of the simulations.

In Table II, we give a summary of the present calculations. This table shows the initial conditions and average properties after the equilibrium periods. In order to investigate the dependence on the system size, we selected the number of particles as 128 and 250. Equilibrium runs were determined from stability of the energy of the system and of the chemical potential of each region (approximately 4000 runs), and after that, the production runs follow (approximately 6000 runs).

Table II. Phase Coexistence Properties of Silicon by the Constant-NVT Gibbs Ensemble

Temperature (K)	Total number of particles	Density of vapor phase ($kg \cdot m^{-3}$)	Density of liquid phase ($kg \cdot m^{-3}$)
7423	128	180.5	1634
6794		47.40	1761
6542		42.27	1816
6290		27.36	1908
6164		25.20	1929
6039		23.90	1959
5913		16.48	1961
5787		15.41	2019
5536		10.75	2040
5284		6.552	2092
5032		3.969	2121
4781		2.870	2172
4529		1.538	2197
4277		0.9557	2238
4026		0.4947	2248
7171	250	84.92	964.5
7045		79.24	1629
6919		71.40	1721
6794		72.81	1788
6542		46.90	1831
5913		18.16	1978
5661		10.60	2001
5032		4.469	2135
3217		0.0470	2348

3. RESULTS AND DISCUSSION

3.1. Vapor–Liquid Coexistence Curve of Silicon

The vapor–liquid coexistence curve of silicon and the coexisting properties of silicon are presented in Figs. 3 and 4 and Table II. In Fig. 3, the phase diagram, along with the line of the law of rectilinear diameters [10], is shown. This line is determined by fitting the points derived from the averages of saturated liquid and vapor densities. At higher temperatures near the critical point, our calculations include large fluctuations as has been observed in numerous studies using the GEMC; therefore, our critical properties should have the error range described below. In Fig. 4, comparisons with experiments are shown. The dashed line represents an empirical formula determined by Lucas [11] for temperatures from 1700 to 1900 K. In order to compare with liquid densities from simulations, the line is extended to high temperatures. Strictly speaking, the experimental condition is not phase equilibria, but the rough comparison will make sense because there is agreement that it is quite near zero pressure. The line on the left in Fig. 4 is a saturation curve based on an empirical formula for vapor pressure [6], and the vapor density line was calculated from the

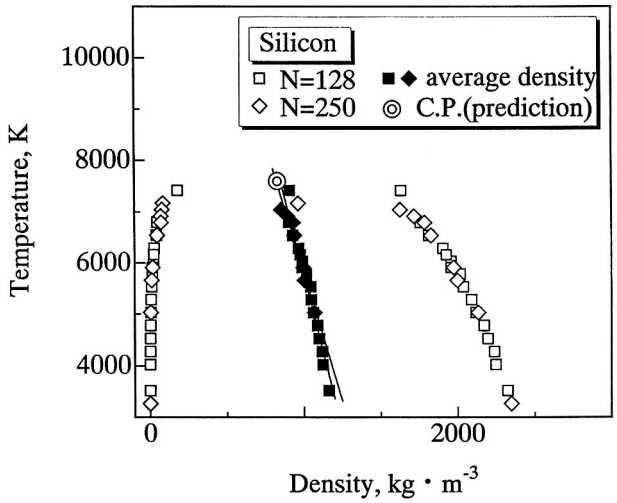

Fig. 3. The vapor–liquid coexistence properties and estimated critical point of silicon. The filled symbols are the averages of the vapor and liquid densities. The lines represent the fitted curves using least squares and the double circle shows our predicted critical point of silicon.

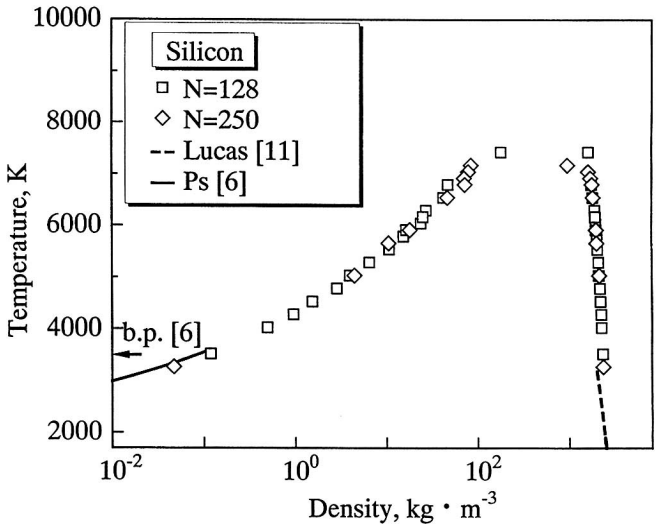

Fig. 4. The coexistence curve compared with experimental data.

formula and the equation of state of the ideal gas: $Pv = RT$. The vapor densities, especially below the boiling point, are very low, and can be almost regarded as an ideal gas. Practically, the values predicted from simulations and the obtained curve show good agreement with each other.

The dependence of the properties on the size of the system should be noted. At low temperatures, the saturated densities and potential energies show little differences between the systems of 128 and 250 particles. This means that GEMC simulations of this system can be performed using less atoms if good initial densities are established. On the other hand, at a temperature of about 8000 K, which is above the estimated critical point, the calculation of the average made no sense due to the frequent phase inversions as pointed out by Panagiotopoulos [4].

3.2. Critical Parameters

To specify the critical point accurately, we attempt to do such not only from the phase diagram but also from another method. The law of rectilinear diameters [10] is one of the techniques that can be used to estimate the critical point of a fluid. It is given as

$$\frac{\rho_L + \rho_G}{2} = \rho_c + A\left(1 - \frac{T}{T_c}\right) \tag{8}$$

Table III. Boiling Points and Critical Points of a Variety of Substances

Substance	Boiling point T_b (K)	Critical point T_c (K)	T_c/T_b
Si (present work)	3650 [6]^a	7800	2.14
Si	3650 [6]^a	5193 [14]^a	1.98
C [12]	—	6800^a	–
SiO_2 [13]	5638^a	11976^a	2.12
NaCl [14]	1734	3300^a	1.90
Ar [15]	87.3	150.9	1.72
H_2O [15]	373.2	647.1	1.73
CH_4 [15]	111.6	190.6	1.71

^{a} Results of calculations, simulations, and estimations.

From the coexistence curve and the law of rectilinear diameters, the critical properties of silicon, $T_c = 7500 \pm 500$ K and $\rho_c = 800 \pm 100$ kg · m^{-3}, are estimated.

In Table III we compare critical point and boiling point temperatures for a variety of substances. The critical point temperatures reduced by their characteristic boiling point temperatures are also shown. It is observed that H_2O, CH_4, etc., form one group at approximately $T_c = 1.7T_b$. However, for the high-temperature melts, such as Si, NaCl, SiO_2, etc., the ratio $T_c/T_b \approx 2.0$, indicating a different group of compounds.

4. CONCLUSION

In this paper, we determined the vapor–liquid coexistence curve of silicon, one of the high-temperature melts. We predicted the vapor–liquid critical point using the GEMC. At low temperatures, the calculated properties showed little dependence on the total number of particles and the calculated values were in agreement with measured values. For the entire range of temperatures, the equality of chemical potentials was demonstrated. From both theoretical and experimental points of view, our calculations were consistent.

REFERENCES

1. M. P. Allen and D. J. Tildesley, *Computer Simulation of Liquids* (Clarendon Press, Oxford, 1987), pp. 110–139.
2. I. Okada and E. Osawa, *The Introduction of Molecular Simulation* (Kaibundo, Tokyo, 1989), pp. 63–80.
3. D. A. Kofke, *J. Chem. Phys.* **98**:4149 (1993).
4. A. Z. Panagiotopoulos, *Mol. Phys.* **61**:813 (1987).

5. A. Z. Panagiotopoulos, *J. Chem. Phys.* **101**:813 (1994).
6. T. Iida and R. I. L. Guthrie, *The Physical Properties of Liquid metals* (Oxford University Press, Oxford, 1988), pp. 85–88.
7. F. H. Stillinger and T. A. Weber, *Phys. Rev.* **31**:5262 (1985).
8. B. P. Feuston, R. K. Kalia, and P. Vashishta, *Phys. Rev. B* **37**:6297 (1988).
9. W. D. Luedtke, M. W. Ribarsky, R. N. Barnett, and C. L. Cleveland, *Phys. Rev. B* **37**:4637 (1988).
10. H. E. Stanley, *Introduction to Phase Transitions and Critical Phenomena* (Oxford University Press, Oxford, 1971).
11. L. D. Lucas, *Mem. Sci. Rev. Metallurg.* **61**:1 (1964).
12. F. P. Bundy, *Mat. Res. Soc. Symp. Proc.* **383**:3 (1995).
13. Y. Guissani and B. Guillot, *J. Chem. Phys.* **104**:15 (1995).
14. Y. Guissani and B. Guillot, *J. Chem. Phys.* **101**:1 (1994).
15. D. R. Lide (ed.), *CRC Handbook of Chemistry and Physics, 77 ed.* (CRC Press, Boca Raton, FL, 1996), pp. 6–54.